Emission Control Science and Technology (2026) 12:16
https://doi.org/10.1007/s40825-026-00297-8

RESEARCH

Time-Resolved Dynamics During the Initial Decline in Catalytic Activity of the CO + NO Reaction over Platinum – Elucidating the Role of NCO

Thomas Häber[1] · Samuel Struzek[1,2] · Lachlan Caulfield[3] · Sui Wan[1] · Florian Maurer[2] · Patrick Lott[2] · Alexei Nefedov[3] · Christof Wöll[3] · Jan-Dierk Grunwaldt[1,2] · Olaf Deutschmann[1,2]

Received: 4 February 2026 / Revised: 10 April 2026 / Accepted: 14 May 2026

Abstract
The reduction of NO by CO over a powdered Pt/Al_2O_3 catalyst in flow reactors is investigated as a function of temperature and stoichiometry at low concentrations typical for emission control. The study investigates the initial decline in conversion over pre-reduced catalysts and its correlation with the formation (and decomposition) of isocyanate (–NCO) on the support, tracked by time-resolved *operando* and *in situ* diffuse reflectance infrared Fourier transform spectroscopy (DRIFTS). Free sites on noble metal particles are necessary for both isocyanate formation and decomposition. CO adsorption and isocyanate formation occur on different time scales, but the amount of isocyanate equilibrates with CO coverage. In the presence of hydrogen, isocyanate decomposes rapidly, producing NH_3. The timescales for -NCO formation and activity decline are similar, suggesting a direct link or influence by a common process. Findings align with models that show a) isocyanate formation might aid NO dissociation by countering the inhibiting effect of CO adsorption, and/or b) changes in the oxidation state affect both catalytic activity and isocyanate formation.

Keywords Catalytic conversion · NO reduction by CO · Pt/Al_2O_3 · Deactivation · Isocyanate formation · Catalyst regeneration · Emission control

1 Introduction

Due to their negative impact on the environment and human health, nitrogen oxide (NO), carbon monoxide (CO), and hydrocarbon (HC) emissions from internal combustion engines and industrial exhaust are of particular concern [1]. Emission standards set by governments have significantly reduced the number of potentially hazardous substances and continue to do so today, further increasing the need for technical solutions to reduce emissions [2]. An example is the three-way catalytic converter (TWC) for spark ignition engines, which has significantly reduced NO_x, CO and HC emissions. Unlike compression ignition engines, industrial exhaust and the exhaust from spark ignition engines often contain sufficient amounts of CO, hydrocarbons and/or hydrogen (H_2) to serve as reducing agents for NO and NO_2 species. Thus, the reduction of NO_x by CO offers a simple and cost-effective technology to decrease NO_x emissions from mobile and stationary sources, with CO acting as the reductant for NO and NO_2 [3–5]. In recent decades, extensive research has been conducted to investigate the performance of noble metal and transition metal catalysts in the reduction of NO by CO for gas purification [5]. Due to rhodium's advantageous effect on activity and selectivity in the CO + NO reaction, rhodium-based catalysts, as well as bimetallic rhodium-platinum catalysts, have been shown to be a crucial component for the reduction of nitric oxide in automobile exhaust [5–8]. This improvement is attributed to the increased ability of metallic rhodium to dissociate NO compared to platinum. Iridium-based catalysts exhibit outstanding activity for NO reduction by CO in the presence

✉ Thomas Häber
thomas.haeber@kit.edu

1 Institute of Catalysis Research and Technology (IKFT), Karlsruhe Institute of Technology (KIT), Hermann-von-Helmholtz-Platz 1, Eggenstein-Leopoldshafen 76344, Germany

2 Institute for Chemical Technology and Polymer Chemistry (ITCP), Karlsruhe Institute of Technology (KIT), Engesserstr. 18/20, Karlsruhe 76131, Germany

3 Institute of Functional Interfaces (IFG), Karlsruhe Institute of Technology (KIT), Hermann-von-Helmholtz-Platz 1, Eggenstein-Leopoldshafen 76344, Germany

Published online: 09 June 2026

of oxygen and also show high resistance to sulfur and water poisoning, making them suitable for industrial use [5]. However, researchers have also investigated other noble or transition metal-based catalysts intensively [4, 5, 9], not least because of the huge increase in the cost and limited availability of rhodium and iridium [10].

One very well-known example is platinum supported on alumina (Pt/Al_2O_3), whose catalytic effect on the reaction CO + NO has been intensively studied for almost five decades, starting with the pioneering work of Unland [11]. Srinivasan and Depcik provide a comprehensive review of the historical development and current state of research on the catalytic reduction of NO by CO using Pt/Al_2O_3, in the absence of other components, such as hydrocarbons, hydrogen, or water [12]. From a mechanistic point of view, and according to the general view in the literature, the reaction involves the non-dissociative adsorption of NO and CO, followed by the dissociation of NO (see [12, 13] and references therein):

$$CO + * \rightleftharpoons CO^* \quad (1)$$

$$NO + * \longrightarrow NO^* \quad (2)$$

$$NO^* + * \longrightarrow N^* + O^* \quad (3)$$

$$CO^* + O^* \longrightarrow CO2 + 2* \quad (4)$$

$$2N^* \longrightarrow N2 + 2* \quad (5)$$

$$NO^* + N^* \longrightarrow N2O + 2* \quad (6)$$

$$O^* + O^* \longrightarrow O2 + 2* \quad (7)$$

Here, * represents an empty site on the catalyst's surface or an adsorbed species. The rate determining step is generally assumed to be the dissociation of NO (Eq. 3), although it is still debated whether the intrinsic dissociation rate or the number of available reduced Pt sites limits the dissociation of NO. The global reaction rate has a negative order at low temperatures (low conversion regime) with respect to the partial pressure of CO [12, 14, 15], implying that CO limits the number of free reduced sites. Thus the global reaction rate will decrease with increasing the CO coverage. Nevertheless, CO does not form impenetrable islands that prevent NO from adsorbing [16–18]. The recombination of adsorbed oxygen atoms to molecular oxygen, Eq. 7, plays a minor role, except at higher temperatures ($> 430°C$) [19].

Platinum (Pt) is a highly active [15] and cost-effective [10] component in the reaction NO + CO, but there are three disadvantages that limit the technical application of bare Pt/Al_2O_3 in technical systems today: 1) It has the highest light-off temperature among the platinum group metals [20, 21]. 2) Depending on operating conditions and stoichiometry, it forms significant amounts of N_2O [14, 15, 21–23], a greenhouse gas with ~ 300 times the global warming potential of CO_2 [1]. 3) Near stoichiometry and under rich conditions (excess CO), the catalytic activity rapidly decreases over time and settles at a much lower level [14, 15, 22, 24]. The exact turning point depends on the actual composition of the mixture and shifts further towards lean conditions with increasing CO concentration [14, 24, 25]. This well-known deactivation behavior and bi-stability of the CO + NO system over Pt/Al_2O_3 [14, 24] is accompanied by the formation of adsorbed isocyanate (–NCO) and adsorbed CO on oxidized platinum sites ($Pt^{n+}-CO$) [11, 22, 25–30]. Isocyanate is probably formed on platinum but quickly spills over to the support. However, the precise role of these species in the reaction mechanism and catalytic deactivation is not generally clear to date [14, 15, 22, 28, 31].

Note that the formation of –NCO is not included in current kinetic models, (1) to (7), as NCO forms rapidly at higher partial pressures of NO and/or CO and is assumed to decompose under real-time operating conditions for catalytic converters ($> 600°C$; reacts with water to form NH_3 and CO_2) [12]. On the other hand, the reduction of NO by CO over Pt/Al_2O_3 is most susceptible to dynamic, oscillatory operating conditions among platinum group metals [21, 27], which could be adjusted to minimize or even eliminate N_2O formation [21]. Under such conditions, and taking into account that the surface composition of all species is fully reversible with respect to changes in the stoichiometry of the feed stream [25, 27], the deactivation and reactivation dynamics will play an important role, especially at the lower limit of operating temperatures. However, until now, only a limited amount of quantitative data on the dynamics of deactivation / reactivation is available, and there is no microkinetic model that describes these dynamics, which must account for the formation of –NCO as an additional sink for NO and CO. Up to date, there has been a lack of studies of the dynamic behavior in the CO/NO system for the development of such models.

Although the formation of isocyanate has been confirmed spectroscopically [11, 22, 26, 28, 30, 32–34], its quantitative dynamics and direct contribution to catalyst deactivation remain poorly understood. Currently, no microkinetic model incorporates dynamic phenomena such as deactivation/reactivation or considers –NCO as an additional sink for NO and CO or as a reaction intermediate. This study addresses this gap by providing time-resolved, quantitative measurements of –NCO formation and decomposition under realistic low-concentration conditions and correlating these processes with catalytic activity decline. Such insights are essential for refining kinetic models and improving emission control strategies.

In previous work, a novel channel reactor enabled spatio temporal correlations between catalytic activity monitored via planar laser induced fluorescence (PLIF) and catalyst oxidation state tracked by *operando* X-ray absorption spectroscopy (XAS) during the reduction of NO by CO over Pt/Al_2O_3 [35]. That study revealed that catalytic activity declines on timescales distinct from changes in Pt oxidation state and suggested that transient isocyanate formation might mitigate CO poisoning by removing CO from Pt sites. However, evidence for NCO involvement was indirect, inferred from spatial gradients and stoichiometric shifts rather than direct detection. The present work builds on these findings by employing *operando* DRIFTS and powder bed reactors to directly observe isocyanate species and quantify their formation and decomposition. Furthermore, a range of inlet conditions is explored, including temperature, stoichiometry, and the presence of H_2 that influence -NCO stability and its potential role as intermediate in the NH_3 formation under exhaust like conditions.

2 Materials and Methods

2.1 Catalyst Preparation

The catalyst was prepared using the CATIMPREG platform (Chemspeed) [36] for automated incipient wetness impregnation and used as reference catalyst in the Collaborative Research Center 1441. A solution of tetraamineplatinum(II) nitrate (Fischer Scientific, 99.99%) diluted in water was added dropwise to a commercial aluminum oxide support (γ -Al_2O_3, Sasol Puralox TH 100/150, calcined for 5 hours at 700°C in static air). Subsequently, the material was dried for two hours at 75°C and a reduced pressure of 120 mbar. After drying, these two steps were repeated eight times in total. Temperature and pressure were controlled by the CATIMPREG platform, while the impregnation process was performed in 12 double-walled glass reactors, similar to [37]. The mixed sample was then calcined for 5 hours at 500°C in static air. The final platinum loading amounted to $1.9 \pm 0.1\%$ as determined by ICP-OES (Inductively Coupled Plasma-Optical Emission Spectrometry) and serves as the reference catalyst in the Center for Emission Control Karlsruhe.

The catalyst was examined by TEM using a Themis 300 Probe Corrected (S)TEM configuration (see supporting information, Fig. 11). The sample was applied to a copper grid using a dry mix method. Images were taken at various magnifications between 120000 and 980000. The average particle size of platinum nanoparticles was determined by measuring the longest diameter of 700 different nanoparticles, yielding an average size of 2.0 ± 0.9nm. Assuming ideal hemispherical nanoparticles [38], this corresponds to a dispersion value of about 56% for platinum nanoparticles. CO chemisorption experiments gave a dispersion value of approximately 52% for two consecutive measurements, which confirmed the TEM measurements. XRD did not show significant reflections for platinum, confirming that no significantly enlarged nanoparticles are present.

2.2 Conditioning

Before each measurement, the catalyst is pretreated/conditioned by: 1) Oxidation with 10 vol.% O_2 in N_2 at 450°C for one hour. 2) Reduction with 5 vol.% H_2 in N_2 at 400°C for two hours. 3) Removal of the remaining hydrogen in the system by purging with pure N_2 (or Ar) at 400°C for at least 30 minutes or until no hydrogen was detected end-of-pipe. Unless otherwise specified, catalyst conditioning was performed before each series of measurements and separately in each of the setups described below.

2.3 Powder Bed Reactor

For powder bed measurements 100 mg of the 1.9% Pt/Al_2O_3 catalyst are pressed, sieved (125 µm - 250 µm sieve fraction), diluted with 1900 mg of SiO_2 (125 µm - 250 µm sieve fraction) and placed inside a quartz tube (inner diameter 8 mm) of a plug flow reactor. Thus, the total amount of Pt in the catalyst bed is approximately ~ 9.6 µmol. At a dispersion of about 56%, this results in about 5.1 µmol platinum surface sites. Quartz wool plugs hold the catalyst bed in place inside the reactor. Heating is provided by a tube furnace, and the temperature is controlled by two thermocouples placed at the beginning and end of the catalyst bed. Individual gases are dosed by mass flow controllers (Bronkhorst) and the total gas flow is set to 1L/min (NTP $\equiv$ 1 atm & 20°C), resulting in a weight hourly space velocity (WHSV) of 32000 L/h/g_{Pt}. Cooling and heating rates are set to 10°C/min. For each catalytic deactivation cycle, a gas mixture of CO and NO balanced by N_2 is fed for one hour and the outlet gas composition is analyzed using an FTIR spectrometer (MultiGas 2030 FTIR Continuous Gas Analyzer, MKS Instruments). Throughout the manuscript, species concentrations in the gas phase are expressed either in ppm, denoting mole per mole (10^{-6} mole/mole), or in percent by volume (volume percent, abbreviated as %). To verify reproducibility, several deactivation cycles with different recovery times (at least 4.5 hours) were performed using a gas flow of 1L/min N_2 to clean/reactivate the catalyst.

2.4 Infrared Spectroscopy

Measurements of diffuse reflectance infrared Fourier transform spectroscopy (DRIFTS) are conducted using

a VERTEX80 FTIR (Bruker) device, which is fitted with Praying Mantis diffuse reflection optics (Harrick) and a liquid nitrogen-cooled mercury cadmium telluride detector (LN-MCT) [39, 40]. The sample is placed as a powder within a high-temperature in situ cell (Harrick) sealed with ZnSe windows. The temperature of the powder is controlled by a heating cartridge beneath the cell and a circulating water system. A Type K thermocouple is placed in the center of the powder bed to monitor the catalyst temperature. To prevent temperature variations in the catalyst bed, 6 mg of the Pt/Al_2O_3 catalyst are mixed with 54 mg α-Al_2O_3 . The utilization of α-Al_2O_3, due to its low surface area, minimizes interaction between the sample and diluent. An IR background spectrum (256scans, resolution of 2 cm^{-1}) of the untreated sample is captured at 25°C under inert conditions. The sample undergoes an oxidative and reductive pretreatment, consistent with the method used for powder bed measurements, to remove organic residues and moisture, which is confirmed through reference spectra recorded both prior to and following the pretreatment.

Once the target temperature is reached, a reference spectrum is recorded with 256 scans and a resolution of 2 cm^{-1} under N_2, serving as the background for the IR absorbance spectra collected during transient measurements. Prior to switching to the specified NO/CO mixture, continuous recording of spectra is started (approximately 2 seconds per spectrum, averaged over 8 scans). The outlet gas composition is evaluated for integral conversion using an FTIR spectrometer (MultiGas 2030 FTIR Continuous Gas Analyzer, MKS Instruments) at the DRIFTS cell's outlet. Spectra are recorded continuously until the IR signals approach saturation. Following each measurement, the sample cell is reheated to 450°C under a flow of pure N_2 to desorb all species from the surface. Heating is continued until all IR bands attributed to surface species disappear. After each heating cycle, it is verified that the IR spectrum has returned to the state observed immediately after the initial oxidative and reductive pretreatment.

Flow rates are controlled by mass flow controllers (Bronkhorst), maintaining a total gas flow of 250mL/min (1 atm & 20°C), yielding a WHSV of 135000L/h/g_{pt}. This WHSV is set higher than that used for powder bed measurements to ensure suitable time resolution and to satisfy the calibration parameters of the end-of-pipe FTIR analysis.

3 Results and Discussion

3.1 Powder Bed Reactor

In an earlier work, we detailed observations of the initial decline in catalytic activity during NO reduction by CO, employing planar laser-induced fluorescence (PLIF) to elucidate catalytic activity over Pt/Al_2O_3 layers with spatial and temporal resolution [35]. The findings were complemented by end-of-pipe measurements obtained in a novel channel reactor, paired with time-resolved X-ray absorption spectroscopy (XAS) measurements at various positions along the plate, enabling monitoring of the temporal and spatial Pt oxidation state evolution as the catalytic activity declined. To corroborate our earlier results, we now report measurements obtained in a powder bed reactor (PBR) under selected operating conditions. The powder bed configuration reduces potential external gas phase transport limitations [41] and more closely mimics the conditions in the DRIFTS cell.

Figure 1 shows the time evolution of catalytic conversion at 300°C for three stoichiometries: net oxidizing (200 ppm CO, left), stoichiometric (400 ppm CO, middle), and net reducing (800 ppm CO, right). The NO feed concentration is kept constant at 400 ppm. In contrast to the channel experiments reported earlier [35], no CO_2 is added to the inlet gas stream to also observe the evolution of CO_2. Additional experiments with and without CO_2 resulted in only marginal differences, comparable to the overall reproducibility of the experiment, which is on average better than 5

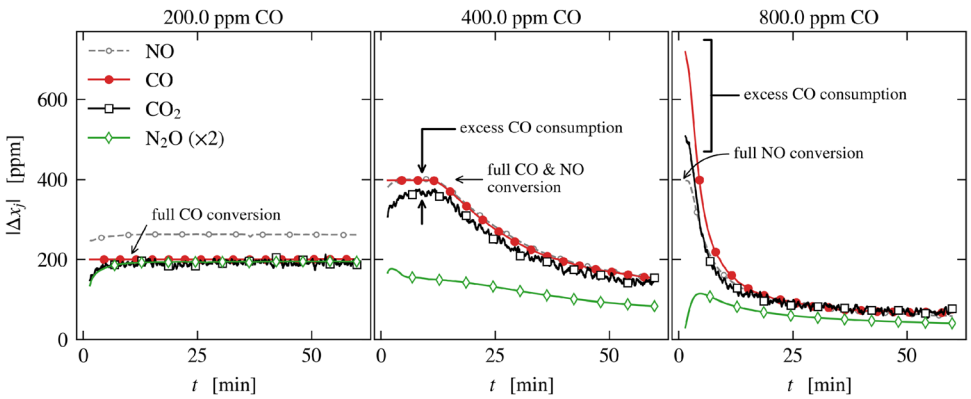

Fig. 1 CO and NO conversion as well as N_2O and CO_2 formation in the powder bed reactor (PBR) at 300°C as a function of time and for three different stoichiometries: net oxidizing (200 ppm CO), stoichiometric (400 ppm CO) and net reducing (800 ppm CO). Total gas flow (1.0 L/min) and inlet NO concentration (400 ppm) are kept constant in all cases

ppm at 200 and 400 ppm CO and better than 15 ppm at 800 ppm CO (see Fig. 12 in the Appendix).

At $t = 0$ min, the feed stream is switched from pure N_2 to the corresponding CO/NO mixture, balanced by N_2. The catalytic conversion $|\Delta x_j|$ depicted in Fig. 1, i.e. the consumption of reactants (CO and NO) or the formation of products (N_2O), is monitored as a function of time, where x_j is the mole fraction of species j and $\Delta x_j = x_{j,out} - x_{j,in}$ is the concentration difference between reactor outlet and inlet. Since the amount of N_2O formed is significantly less than the initial conversion of CO or NO, the formation of N_2O in Fig. 1 has been multiplied by a factor of two to better visualize the temporal evolution. The response time of the FTIR signal to a sudden and abrupt change in inlet concentrations is approximately 15 s and is mainly due to the size of the FTIR gas cell (200 mL), the flow rate and volume of the reactor tube (inner diameter 8 mm, length 750 mm) and the associated residence time after a step change in concentration (see Fig. 13 in the Appendix). To avoid artifacts in the calculation of the catalytic conversion, the first 60 seconds were therefore excluded from all measurements.

Starting with a preconditioned catalyst, each measurement is repeated four times by purging the catalyst bed with nitrogen at 300°C for at least 4.5 hours after each conversion cycle. The high reproducibility of these cycles (compare Fig. 12) indicates that the original catalytic activity of the preconditioned (reduced) catalyst can be restored simply by flushing with inert gas [14], suggesting that the deactivation is reversible, that is, it can be reversed by thermal desorption or decomposition of the species responsible for the reduced activity.

Under net oxidizing conditions (Fig. 1, left), CO undergoes complete conversion from the very start, whereas NO consumption and formation of N_2O and CO_2 increase modestly in the first minutes before remaining constant throughout the measurement period. Later ($t > 10$ min), CO consumption and CO_2 formation are very close to each other, indicating that almost all CO is converted to CO_2. Initially ($t < 10$ min), however, less CO_2 is formed than would be expected based on the amount of CO consumed.

Analogous observations, but to a much greater extent, are found under stoichiometric and net reducing conditions. At 400 ppm CO (stoichiometric), both NO and CO are fully converted in the first 12 minutes, followed by a slow decline in catalytic activity. The system does not reach steady state even after 60 minutes. It should be noted that CO_2 formation is significantly lower than CO consumption during the entire measurement period. Since CO is the only carbon source, some CO must be converted to a species other than CO_2, resulting in a carbon deficit at the reactor outlet. The initial discrepancy between CO_2 formation and CO consumption is even larger under net reducing conditions (800 ppm CO), however, the carbon imbalance disappears after about 20 minutes. During all this time, the conversion rate decreases, and the system almost reaches steady state after 60 minutes. The decrease in NO and CO conversion, once it starts, is faster at higher CO concentrations.

Two further observations at 800 ppm CO merit discussion. First, the CO conversion far exceeds the NO conversion in the first 20 minutes. Initially, the CO turnover frequency is almost twice the NO turnover (by a factor of ~1.8). At 400 and 200 ppm CO, carbon monoxide is the limiting component, therefore excess consumption of CO over NO is difficult to detect. [15] also reported a higher CO consumption compared to NO consumption during the decline in catalytic conversion, whereas the opposite would be expected if only N_2 and N_2O are formed. Similarly, [22] observed an excess formation of CO_2 compared to the formation of N_2 and N_2O. Based on stoichiometric considerations and supported by IR studies, these effects were attributed to the reaction of one NO with two CO to form -NCO and CO_2. The excess consumption of CO, as well as the excess formation of CO_2 was observed only during the decline in catalytic conversion and disappeared as the systems approached steady state [15, 22]. Therefore, both the carbon deficit and the excess consumption of CO in our measurements can be attributed to the well-known formation of isocyanate above 200°C [30–33, 42–44]. Second, even CO_2 formation exceeds NO consumption during the first 5 minutes by as much as 100 ppm in the beginning, while even more CO is consumed, suggesting that NO is not the only source of oxygen in the system. This could be attributed to the catalyst not being completely reduced by H_2 initially, as confirmed by XAS measurements [35].

After dissociation of NO^* into N^* and O^* (2), adsorbed nitrogen can react with CO^* to form NCO^* and migrate to the support as –NCO:

$$CO^* + N^* \rightleftharpoons NCO^* \tag{8}$$

$$NCO^* \rightleftharpoons -NCO \tag{9}$$

Although NCO^* most likely forms on platinum sites, it quickly spills over onto the support (–NCO, 9 [30–33, 42–44], where it is much more stable [11, 33]. By comparison, NCO^* on Pt(110) and Pt(111) decomposes rapidly above 100°C to N_2 and CO [17, 44–46]. The left-over O^* from the NO^* dissociation may react with another CO^* to form CO_2 according to (4). In our experiments, there is no evidence of NO_2 formation ($O^* + NO^* \longrightarrow NO2^*$), consistent with the literature [12]. Consequently, for each NCO^* formed at the surface, an additional CO is consumed by the O^* left over from NO^* dissociation. Stated differently, NCO^* formation consumes two CO for each NO, while it is the reverse for

N_2O formation [22]. Such over-consumption of CO relative to NO is clearly seen in the measurements in the powder bed reactor at 800 ppm CO, cf. Figure 1 (right).

In the following, we will assume that the formation of –NCO is the only process involving carbon-containing species, in addition to the adsorption of CO at the Pt sites and the formation of CO_2 as a product that is rapidly desorbed. In fact, so far there is no evidence from infrared studies of the formation and accumulation of other species [11, 22, 26, 28, 30, 32–34]. In this case, each stored molecule contains only one carbon atom, and the amount of carbonaceous species stored can be estimated from the carbon mass balance between the inlet and outlet of the reactor, integrated over time:

$$n_{C,total}(t) = \int_0^t \dot{n}_C(\tau)d\tau = -\int_0^t [\Delta x_{CO}(\tau) + \Delta x_{CO2}(\tau)]\,\frac{p\dot{V}}{RT}d\tau \qquad (10)$$

where $\dot{V}$ is the volumetric flow rate at pressure p and temperature T, R is the ideal gas constant, and $\Delta x_j = x_{j,out} - x_{j,in}$ is the difference between inlet and outlet concentrations (here expressed as mole fraction) of species j. All experiments in this work were performed under isothermal conditions. The heat of reaction and reaction induced density changes are negligible at the low concentrations used here.

Figure 2 shows the evolution of the total amount of stored carbon-containing species $n_{C,total}$ as a function of time under lean, stoichiometric, and rich conditions according to (10). The error bars correspond to the standard error 1σ of the repeated catalytic cycles, mainly reflecting the reproducibility of the measurements. To account for possible correlations between CO and CO_2 in the MKS FTIR analyzer [47] and to provide a lower bound for the amount of stored -NCO, the carbon imbalance is assumed to be zero at the end of each measurement cycle.

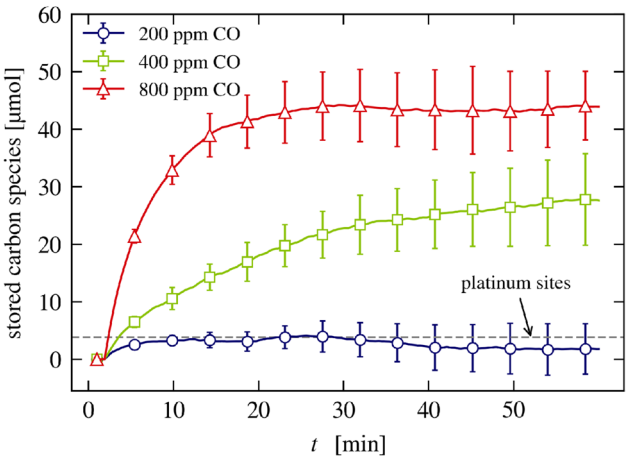

Fig. 2 Estimated minimal amount of carbon species stored $n_{C,total}$ up to time t according to (10) in the powder bed reactor at 300°C. The gas flow rate (1.0 L/min) and inlet NO concentration (400 ppm) are kept constant in all cases and only the CO inlet concentration is varied. The dashed line indicates the estimated number of available Pt sites (5.1 µmol)

Under net oxidizing conditions, the accumulation of -NCO is minimal, if present at all, especially when considering the estimated error margins and the slight deviation of the carbon balance from zero. Conversely, $n_{C,total}$ increases continuously under stoichiometric conditions (apparently even after one hour), while it reaches a plateau after about ten minutes under reducing conditions. In both cases, the total amount of deposited species exceeds the estimated number of available platinum sites, namely 5.1 µmol, represented by the horizontal dashed line in Fig. 2, determined based on the platinum loading and dispersion). This statement remains true even when taking into account the significant margins of error in the absolute values. γ-Al_2O_3 has a remarkable adsorption capacity for HNCO of 2200 µmol/g (at room temperature), which is dissociatively adsorbed on transition metal oxides [48]. This high storage capacity is in large part the result of the high surface area of γ-Al_2O_3 compared to other transition metal oxides. Based on the specific surface area and the amount of catalytic sample used for the powder bed measurements, we can estimate the storage capacity at room temperature to be on the order of ~170 µmol. Taking into account the decrease in storage capacity with temperature and the uncertainty in these estimates, the storage capacity is larger but of a similar order of magnitude to the –NCO storage observed in the powder bed measurements.

Indirect evidence that there is a large surplus of adsorbed –NCO compared to the number of platinum sites available has already been obtained from IR measurements of adsorbed species [30, 32, 33]. Together with the observation that the IR absorption frequency of adsorbed isocyanate is largely independent of the noble metal but sensitive to the support material [30, 43, 48], these were clear indications of a rapid accumulation of isocyanate on the support. Our results in Fig. 2 are consistent with these earlier findings. They provide a quantitative measurement of the amount and time evolution of –NCO storage on Pt/Al_2O_3 under operating conditions and emphasize that the formation rate of –NCO is strongly dependent on experimental conditions.

3.2 DRIFTS – NCO Formation

The powder bed results in the previous section indicate that -NCO is formed and stored on the surface of the support. Although the evidence is indirect through the observed carbon imbalance, it is consistent with previous literature [30–33, 42–44]. Moreover, the time scale of the changes in carbon imbalance matches that of the decline in catalytic activity, and there appears to be no carbon imbalance once

the system reached steady state [15, 22, 29]. So, it appears that both processes are connected or that the process responsible for the decline in catalytic activity also influences the formation of -NCO. The transient DRIFTS measurements presented in the following section first provide direct evidence for the formation of -NCO under the conditions selected here, with very low concentrations of NO and CO. However, a particular focus is on gaining insight into the dynamics of the formation of –NCO.

The measurement procedure is very similar to that described above for powder bed measurements. After pretreatment, the sample is cooled under N_2 to the desired reaction temperature, at which a reference spectrum is obtained and continuous DRIFTS scans are started. At $t_0 = 0\,\mathrm{min}$, the catalyst is exposed to a gas mixture of CO and NO, balanced by N_2 at a total flow rate of 250 mL/min. Simultaneously, the effluent gas composition at the outlet is monitored by FTIR spectroscopy to record the time-dependent integral conversion. A typical DRIFT spectrum obtained after 8 min under stoichiometric conditions at 300°C is shown in Fig. 3.

The most striking feature is the asymmetric stretch vibration band of –NCO at 2261 cm^{-1}, which agrees well with the values reported in the literature for -NCO on the Al_2O_3 support [11, 27, 28]. The spectral region between 2080 and 1900 cm^{-1} is attributed to CO molecules adsorbed in a linear configuration on metallic platinum. Specifically, the CO band at 2069cm^{-1} is characteristic of CO adsorption on highly coordinated Pt sites of Pt nanoparticles. In contrast, the low-wavenumber tail likely arises from CO bound to various under-coordinated sites on small Pt clusters as well as to platinum–ceria interfacial sites in a bridging configuration [49]. Other bands frequently reported in the literature for this system (e.g., at 1630, 1564, and 1474cm^{-1}) are usually attributed to nitrite and nitrate species.

The broad band between approximately 3000 cm^{-1} to 3700 cm^{-1} can be attributed to the formation of H-bonds between the hydroxyl groups on the support and the adsorbed species, probably -NCO, with the complementary depletion of the free OH group at 3765 cm^{-1}. However, there is only one dominant negative OH band, corresponding to only one of the three known Lewis acid cites on the γ -alumina surface [50, 51]. The OH groups of the other two Lewis acid sites, which are commonly observed near 3729 and 3671 cm^{-1}, produce only very weak signals, if any.

In terms of temporal evolution, the degradation of the free OH group, the emergence of H-bonded hydroxyl species, and the nitrite/nitrate bands all scale independently of the stoichiometry relative to the intense –NCO band (see also Fig. 15). This behavior corroborates previous findings on barium-containing lean NO_x trap catalysts [52], indicating that these processes are associated with the storage of isocyanate at Lewis acid sites on the support. As an illustrative example, Fig. 4 shows the temporal evolution of the DRIFT spectrum under stoichiometric conditions, at 300°C in the range 1300 cm^{-1} to 2400 cm^{-1}. At $t = 0\,\mathrm{min}$, the intensity of –NCO begins to increase with time and reaches a nearly steady state after about 10 min. The same behavior is observed for the bands associated with nitrite/nitrate species. In contrast, the Pt-CO band appears almost immediately and remains constant throughout the measurement period.

To further highlight the qualitative differences in the timescales, Fig. 5 compares only the evolution of the peak intensities of the –NCO and Pt-CO bands for different temperatures and for the same three stoichiometries used in the powder bed measurements. The Kubelka-Munk transformation has been used to more accurately reflect the quantitative

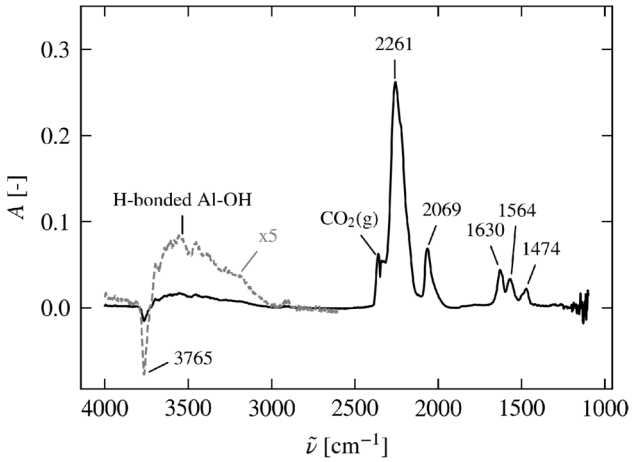

Fig. 3 Typical DRIFT spectrum obtained after 8 min during the reduction of NO by CO. Clearly visible are the asymmetric stretch vibrational band of Al_2O_3-NCO at 2261 cm^{-1} and the Pt-CO band at 2069 cm^{-1}. See text for more details. (300°C, 400 ppm CO, 400 ppm NO, 250 mL/min)

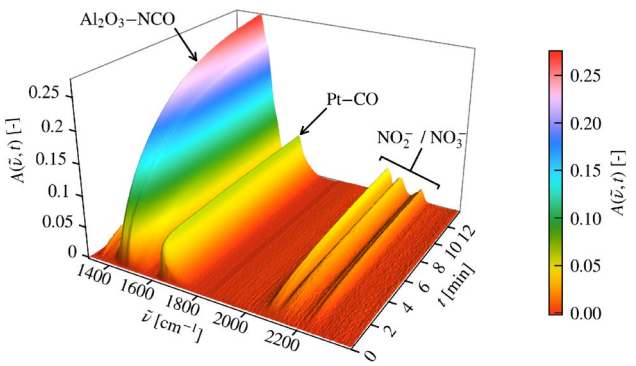

Fig. 4 Temporal evolution of the DRIFT spectra in the region 1300–2400 cm^{-1}, with the absorbance A(v,t) represented by a color scale. The –NCO increases until it reaches steady state after several minutes, whereas the Pt-CO band appears instantly and remains constant. (300°C, 400 ppm CO, 400 ppm NO, 250mL/min)

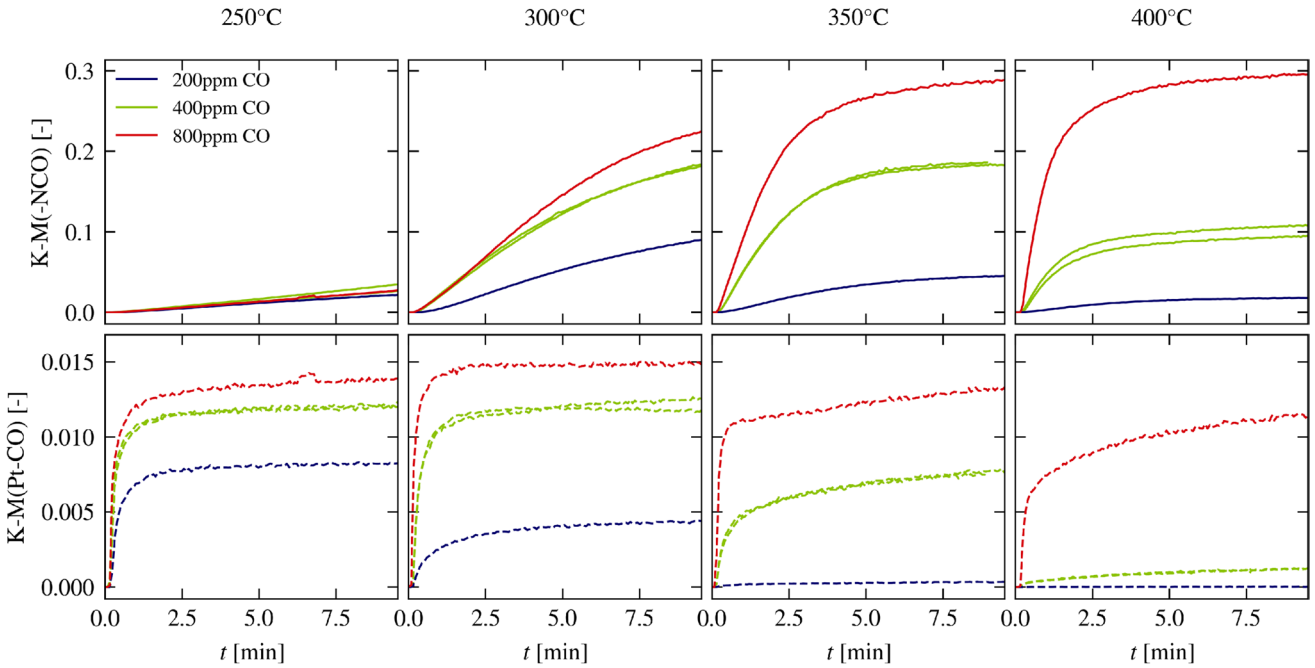

Fig. 5 Development of the peak intensities of the -NCO band at 2261 cm^{-1} (top) and the Pt-CO band at 2069 cm^{-1} over time, measured at different temperatures and for three different stoichiometries. Otherwise, the conditions are the same as in Fig. 4. The Kubelka-Munk transformation has been used to more accurately reflect the quantitative species concentration

species concentration [53]. Herein, we use peak absorption instead of the area under the peak here because the focus is on time-dependent behavior and qualitative differences in intensities. The use of peak absorption is justified as no change in peak width as a function of time at a given temperature is observed, and the overlap between the two spectral features is small. The latter becomes only slightly relevant at higher temperatures.

A comparison of the temporal behavior of the two bands reveals several noteworthy points:

1. Pt-CO almost reaches its saturation intensity within the first few scans, regardless of temperature and stoichiometry, and then remains constant throughout the measurement. The slight increase observed at higher temperatures is due to temperature-induced line broadening and the resulting slight overlap with the –NCO feature (see above).
2. Under net oxidizing (200 ppm CO) and stoichiometric (400 ppm CO) conditions, the intensity of Pt-CO decreases with increasing temperature. At 400°C, the intensity of Pt-CO is greatly reduced or close to zero. However, with an excess of CO (800 ppm), the Pt-CO band, which is an indicator of CO coverage, decreases only slightly with increasing temperature, is still very pronounced at 400°C and comparable in intensity to lower temperatures (see also Fig. 14).
3. There appears to be a correlation between the saturation intensities of –NCO and Pt-CO – the higher the CO coverage, the higher the final amount of isocyanate – which is consistent with the general assumption that the isocyanate on the support (-NCO) is in equilibrium with Pt-CO (cf. Eqs. 8 and 9) [11, 29].
4. The temporal evolution of –NCO and Pt-CO is decoupled from each other. Whilst isocyanate increases over a period of minutes to several dozen minutes depending on the temperature, the CO band and thus the CO coverage appear to remain virtually unchanged as a function of time. The observed increase in Pt–CO band intensity at elevated temperatures can be attributed to the onset of spectral overlap with the –NCO band, arising from temperature-induced broadening of the absorption lines.

Relating the time-dependent formation of isocyanante with the decline in catalytic activity is not straightforward. First, the time resolution of the DRIFT spectra and that of the end-of-pipe concentrations are very different, mainly because of the size of the FTIR gas cell in combination with the smaller volumetric flow rate compared to the powder bed measurements. Second, the DRIFT spectra reflect only the initial (upstream) portion of the catalytic bed, whereas the end-of-pipe data measure the integral conversion. Consequently, any changes along the catalytic bed will not be reflected by the DRIFT spectra. However, previous studies show that

under similar reaction conditions and depending on the stoichiometry, spatial gradients of both catalytic activity and oxidation state occur [35].

To illustrate this challenge, Fig. 6 shows the change in NO and CO concentrations at the outlet of the DRIFTS cell. Some of the time resolution is recovered by deconvolution of the FTIR signal with the residence time distribution of the FTIR cell, using a fast iterative soft-thresholding algorithm [54] implemented in python through the *pylops* package [55] with a penalty on the L_1 norm. The residence time distribution is obtained as the gradient of the FTIR signal response to a step-change in the inlet concentration [56]. Since deconvolution is an ill-posed mathematical problem, it inevitably introduces additional "noise" to the FTIR data. To focus on the decline in activity over time, Fig. 6 just shows the change in concentration, namely $x_j(t) - x_j(t')$, where x_j is the mole fraction and t' corresponds to the time of the first data point in the graph. The first 30 s of the data are discarded from the data, to omit data points dominated by the early rise in concentration in the FTIR when switching from inert gas to the gas mixture containing NO and CO.

A decline in catalytic activity (increase in NO and CO at the outlet) over time is clearly visible for all temperatures. Compared to the powder bed measurements, the decline occurs on a much shorter time scale, mainly due to the much smaller amount of catalyst used in the DRIFTS cell (6 mg vs. 100 mg). Qualitatively, both the DRIFTS cell and the powder bed measurements show similar trends. At 200 ppm CO there is barely any deactivation, while the overall magnitude of change is the largest with an excess of CO (800 ppm). However, there is no obvious trend in terms of faster deactivation with increasing temperature, which would directly correlate with the increasing formation rate of isocyanate seen in the DRIFT spectra. This highlights the deficiencies of the current *operando* DRIFTS approach in time-resolved studies, where the surface-sensitive and gas phase-sensitive methods differ greatly in spatial and temporal resolution.

3.3 DRIFTS – NCO Decomposition

[11] suggested that -NCO might decompose by reacting with adsorbed NO to form N_2 and CO_2. This was already questioned by [29], who observed that -NCO was quite stable in the presence of NO. Instead, a rapid decline of the -NCO band in the presence of water and N_2O was reported. Therefore, and to complement the studies on isocyanate formation in the previous section, we investigate in the next step the decomposition dynamics of –NCO in the presence of several gas species.

As stated previously, the high initial catalytic activity of Pt-Al_2O_3 in the reduction of NO by CO can be restored simply by purging the system with N_2 for some hours at elevated temperature. In accordance with this, we observe a decrease in the intensity of the -NCO band under inert gas. Hence, there seems to be a possibility to thermally decompose –NCO in the absence of NO and CO. To investigate

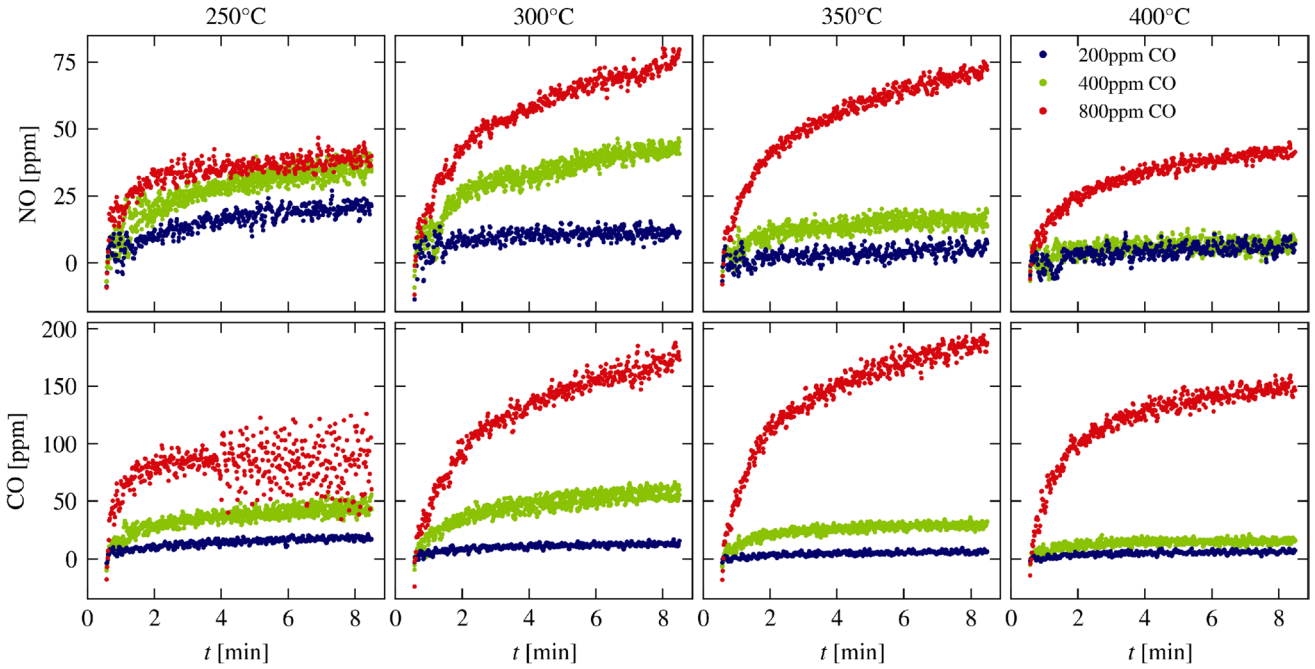

Fig. 6 Change in the NO and CO concentration, $x_j(t) - x_j(t')$, at the outlet of the DRIFTS cell over time, where x_j is the mole fraction and t' corresponds to the time of first data point in the plot. The lower temporal resolution of the FTIR spectrometer was compensated for by deconvolution with the residence time distribution (see text for details). The conditions are the same as in Fig. 5

this process in greater detail, the sample in the DRIFTS cell is first loaded with -NCO and an excess of CO (800 ppm CO, 400 ppm NO) at 350°C. The cell is then cooled to 150°C while maintaining the reaction mixture, and flushed with pure nitrogen to remove adsorbed CO and NO as far as possible. Finally, the DRIFTS cell is heated to 600°C within 4 minutes and DRIFT spectra are continuously recorded during the decomposition.

The associated DRIFT spectra and gas phase concentrations at the DRIFTS cell outlet are presented in Fig. 7. The figure illustrates the time-dependent DRIFT spectra between 1300 cm^{-1} to 2500 cm^{-1} as a 2D image. Moreover, it includes individual spectra at specific times, the temporal evolution of peak absorbances of –NCO and Pt-CO, concentrations of gas phase species at the cell outlet, and the temperature profile. Note that the temperature profile serves as a reference due to inevitable temperature discrepancies between the heating element and the sample at the rapid heating rate employed. Initially, the DRIFT spectra exhibit standard features of –NCO on the support (approximately 2261 cm^{-1}) and bands for nitrites/nitrates, without the presence of Pt-CO (around 2069 cm^{-1}). After approximately 1 min (near 250°C), the intensity of the –NCO band begins diminishing. Concurrently, the Pt-CO band appears and does not vanish until –NCO has largely decomposed. Primarily, CO is noted as a decomposition product at the cell outlet, confirming earlier results by [30], while NO and N_2O occur in trace amounts. The reappearing Pt-CO during decomposition hints that -NCO breaks down into N^* and CO^* on the noble metal; see Eq. 8. CO^* may desorb, allowing two N^* to recombine into N_2, undetectable by FTIR.

In the preceding section, the rapid breakdown of –NCO was achieved by a rapid heating rate, which facilitates the detection of decomposition products due to their pronounced concentrations at the cell outlet. In contrast, under isothermal decomposition within the temperature range of 250 to 400°C, product concentrations typically drop to lower levels of ppm. Therefore, in the following discussion, we concentrate on the temporal variations in the DRIFT spectra and the impact that NO, O_2, CO, and H_2 have on the decomposition rate. The isocyanate is deposited as before at 350°C with 800 ppm CO and 400 ppm NO until the -NCO band nearly reaches full saturation. At $t_0 = 0\,\mathrm{min}$, the gas flow is switched to mixtures comprising pure N_2, 400 ppm NO in N_2, 10% O_2 in N_2, 800 ppm CO in N_2, or 5% H_2 in N_2, respectively, maintaining a constant temperature of 350°C. Unlike the aforementioned rapid thermal decomposition, the system is not purged with nitrogen before switching, so that the response of the Pt-CO band can also be observed. The relevant DRIFT spectra, focusing exclusively on the –NCO and Pt-CO bands, are depicted in Fig. 8; spectra recorded at different times are marked with a color scale. Only every 10^{th} spectrum is shown in the figure, so the time interval between each spectrum is approximately 45 seconds.

The response of the –NCO and Pt-CO bands to different gas mixtures is described separately for each gas composition below.

– N_2: In the presence of pure N_2, the intensity of the –NCO band decreases to about one-third of its initial value within 10 min, with the rate of decrease progressively slowing over time. Extrapolating these time scales suggests that complete removal of –NCO from the surface would require several hours of purging with N_2 at 350°C. This is consistent with the aforementioned observation that activity can be restored by simply purging with inert gas, and indirectly points once again to a connection between the change in activity over time on a freshly reduced catalyst and the formation of –NCO. The decrease in the Pt-CO band intensity occurs in two

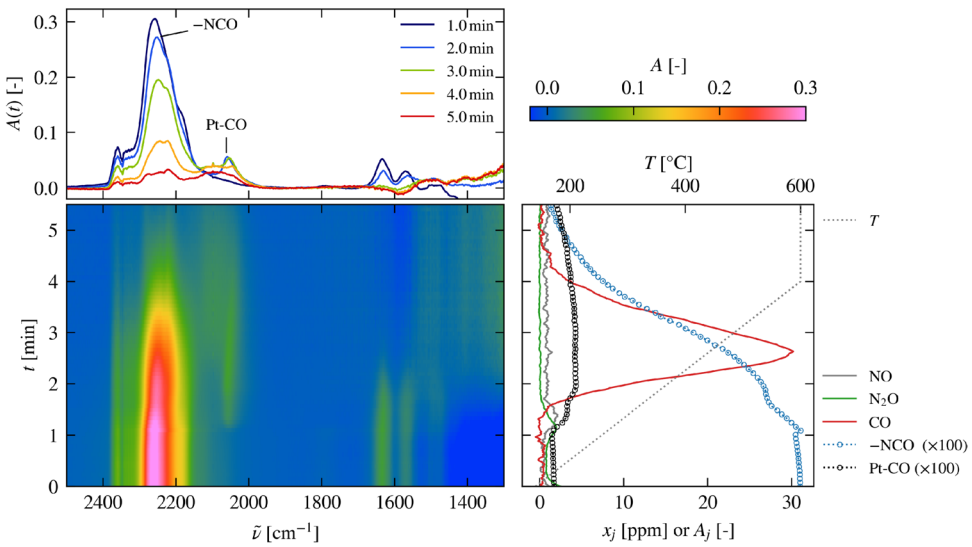

Fig. 7 2D time-dependent DRIFT spectra between 1300 cm^{-1} to 2500 cm^{-1} are shown during flushing with N_2 while heating. This includes spectra at specific times (top), peak absorbance changes for -NCO and Pt-CO, outlet gas species concentrations, and temperature profile (right). Refer to the text for further details

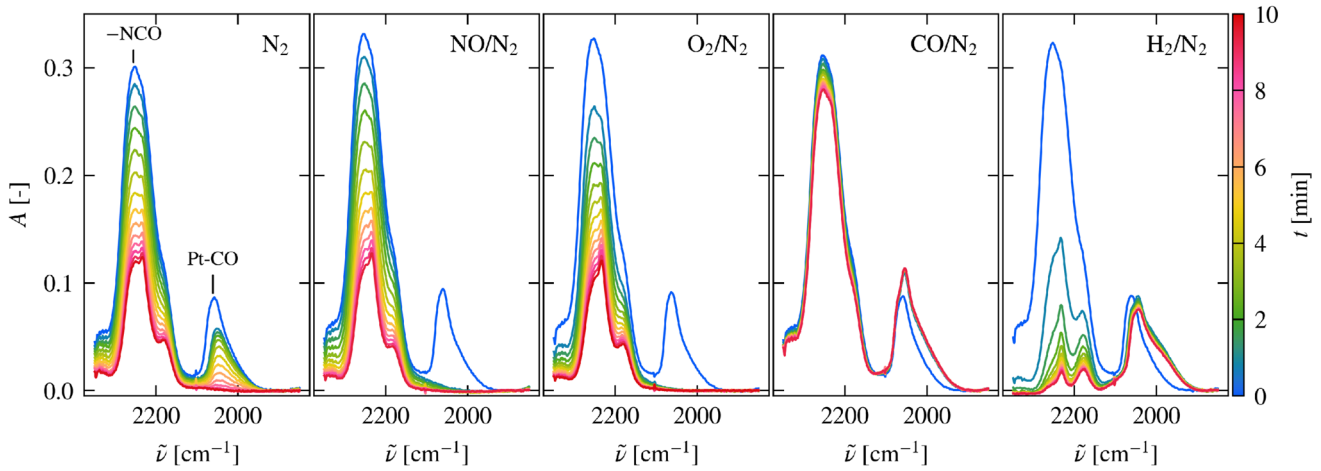

Fig. 8 Evolution of DRIFT spectra in the NCO and Pt-CO bands observed when switching from a CO/NO mixture to gas mixtures with either N_2 or NO, O_2 CO, H_2 in N_2. Temperature and flow rate remain constant at 350°C and 250 mL/min

distinct steps: first, the component at 2069 cm^{-1}, corresponding to CO adsorbed on high-coordinated Pt atop sites, vanishes rapidly in less than 1 min; second, the remaining portion of the band diminishes quickly and disappears entirely after approximately 10 min.

– **NO**: The decrease in isocyanate band intensity in a mixture containing 400 ppm NO in N_2 closely matches that observed in pure N_2, both in magnitude and in rate. Thus, the presence of NO as an oxidizing agent does not seem to enhance the decomposition of NCO, consistent with the findings of [29]. In contrast, the entire Pt-CO band disappears very rapidly, because any CO formed by the decomposition of NCO reacts immediately with NO to yield CO_2, N_2, and possibly also N_2O.
– O_2 : With 10% O_2, the same behavior is observed as in the presence of NO. The decrease in NCO band intensity proceeds with identical time-scales for both oxidizing agents. The same holds for Pt-CO, which is immediately oxidized to CO_2. At the temperature of 350°C used here, oxygen readily dissociates on platinum [19]. Apparent surface saturation or oxidation by oxygen thus does not affect the decomposition rate of –NCO, which remains identical to that of pure thermal decomposition, even in the presence of oxidizing species such as NO and O_2.
– CO: With 800 ppm CO in N_2, the situation is entirely different. Over the course of the measurement, only a very slight decrease in the NCO band is observed, while the Pt-CO band shows an immediate increase in intensity, accompanied by a redshift of its maximum and a subtle change in band shape. These alterations in the Pt-CO band indicate complete saturation of the active Pt sites with CO, in equilibrium with the gas phase CO concentration. The occupation of all Pt active sites by CO molecules accounts for the absence of any significant reduction in the –NCO band. This finding supports the conclusion that not only isocyanate formation [30] but also its decomposition requires the presence of the noble metal particles.
– H_2: When the gas feed is switched to a mixture of 5% H_2 in N_2, the behavior changes again. Within the first two minutes, the NCO band decays very rapidly and almost completely. Simultaneously, the Pt-CO band instantaneously shifts to lower frequencies, with an intensity and shape that closely resemble those of a fully saturated Pt-CO surface in 800 ppm CO in the gas phase (see Fig. 9 for an enlarged view of the Pt-CO band under CO/N_2 and H_2/N_2 at higher temporal resolution). As the process proceeds, the band intensity decreases only slightly, while the spectral features continue to shift toward lower wavenumbers. This temporal evolution is coupled to the decrease of the NCO band and ceases once the latter has nearly vanished. The band at $\sim$ 2050 cm^{-1} remains clearly visible, with an intensity comparable to that of the initial Pt-CO, even after almost complete decomposition of –NCO. It appears unlikely that CO is still bound to Pt at this stage, because once –NCO is consumed, CO would be expected to desorb on a similar timescale as under pure N_2, which is not observed here. Instead, the final band position and shape more closely resemble the infrared spectrum of platinum hydride (Pt–H), both multiply and linearly coordinated, with the relative contributions depending on the experimental conditions [57]. The observed temporal evolution may reflect an electronic restructuring of the Pt surface [57]. The similarity between the DRIFTS bands immediately after initiating the reaction of –NCO with H_2 and those measured under CO in N_2 suggests that the noble-metal surface is initially saturated with CO. As –NCO disappears, the CO source is removed, and the system undergoes a transition from Pt–CO to Pt–H.

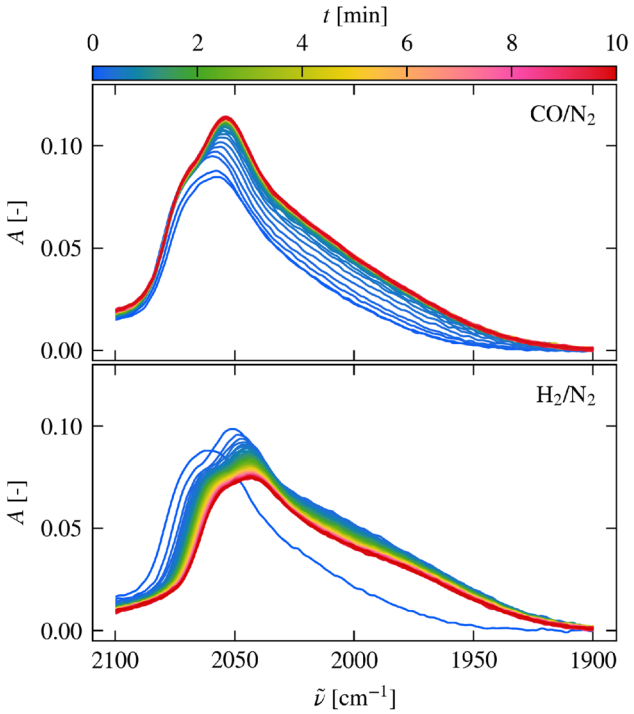

Fig. 9 Transient IR spectra in the region of the Pt-CO obtained after switching from the reactive gas mixture containing $CO/NO/N_2$ to mixtures containing just CO or H_2 in N_2

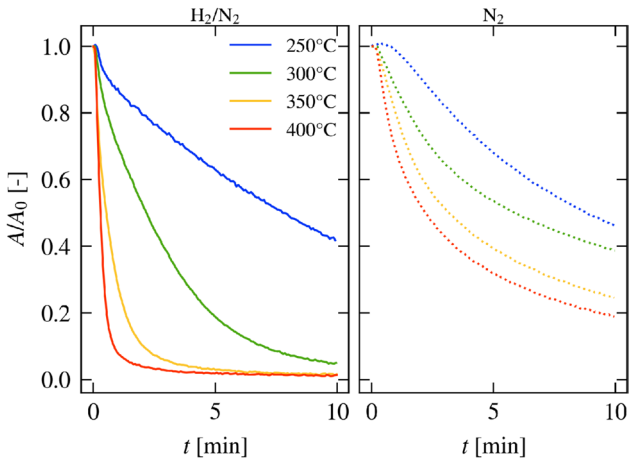

Fig. 10 Decrease in peak absorbance of the –NCO band at ~ 2261 cm^{-1} over time after switching from a CO/NO gas mixture to either 5% H_2 in N_2 (left) or only N_2 (right) at various temperatures, with a constant flow rate of 250 mL/min

A significantly faster decomposition of NCO in the presence of hydrogen, as compared to thermal decomposition under an inert gas (N_2), is evident across all temperatures. This phenomenon is clearly illustrated in Fig. 10, which provides a comparative analysis of the temporal progression of the peak absorption of NCO at ~ 2261 cm^{-1} in environments containing 5% H_2 versus those in pure nitrogen. As anticipated, the rate of purely thermal decomposition in N_2 increases with increasing temperature. At 250°C, the decomposition rate in 5% H_2 is very similar to that observed in the absence of hydrogen. The minor discrepancies can be attributed in part to the variation in catalyst samples utilized during the measurements. Nevertheless, with rising temperature, the remarkable reactivity of –NCO in the presence of H_2 is visible in its rapid decomposition rate.

4 Discussion

There is general consensus in the literature that at high CO concentrations and after reaching steady state, the so-called extinguished state, catalytic conversion is inhibited mainly by high surface coverage of strongly adsorbed CO*, effectively limiting NO* dissociation due to a lack of free reduced sites [12, 14, 15, 24]. The negative reaction order of the global steady-state conversion rate with respect to the CO partial pressure also illustrates this [12, 15, 22]. [29] performed simultaneous activity and IR studies and concluded that the formation of isocyanate proceeds in parallel to the decrease in catalytic conversion. In addition, [22] as well as Granger et al. [15] showed that the transient stoichiometric imbalance and excess CO consumption, both caused by the formation of –NCO, occur only during the initial decline in catalytic conversion and disappear as the system approaches steady state. The combination of time-resolved powder bed and *operando* DRIFTS measurements presented here is in line with those earlier observations, strongly supporting the notion that the decline in catalytic activity and the storage/formation of NCO are correlated.

What role NCO* and NCO play in the catalytic deactivation in the reaction of CO with NO over Pt/Al_2O_3 is still controversially discussed in the literature [14, 15, 22, 27, 28, 31]. According to [22], the accumulation of –NCO groups next to platinum particles may alter their electronic properties, which in turn may affect their activity. [28] attributed the deactivation to the formation of strongly adsorbed CO on oxidized platinum sites (Pt^{n+}–CO) in parallel with –NCO formation, but somewhat delayed, which no longer participate in the reaction and continue to block adsorption sites. This corroborated earlier findings by [27], where the frequency response of the overall conversion under cyclic operating conditions matches that of the buildup and decay of the infrared bands of surface –NCO, but it even slightly better matches that of CO on oxidized Pt sites. [14] were the first to argue that isocyanates have an activating rather than a deactivating effect. Isocyanate formation maintains some NO and CO consumption and extends the time for the catalyst to reach the steady, extinguished state, but otherwise has no effect on catalytic activity. The observation that catalytic

activity can be temporarily increased again by oxidizing or hydrolyzing –NCO points in a similar direction [29].

Under near stoichiometric or under reducing conditions, there is likely an excess of CO* relative to N*, which promotes the formation of NCO*. Rapid spillover onto the support, where –NCO is much more stable [11, 33], removes N* from the surface before it can react with NO* or another N* to form N_2O or N_2. The remaining O* left over from the dissociation of NO* may react rapidly with the abundant CO*. In effect, the formation of isocyanate might effectively counteract the inhibiting effect of CO by partially removing both N* and CO* from the surface. Our results are consistent with such a model, although one cannot completely exclude the possibility that –NCO formation also ceases (in part) due to other inhibitory effects, such as the formation of Pt^{n+}–CO [28].

During rapid decomposition in a hydrogen atmosphere, particularly at elevated temperatures, the predominant product is NH_3, whereas only trace amounts of CH_4 are detected (data not shown). Water is also observed, likely originating from the reaction of H_2 with –NCO species or residual surface hydroxyl groups on the support. The formation of NH_3 during the fast reaction of –NCO with H_2 corroborates the existence of a rapid hydrolysis pathway to NH_3 in SCR systems when NO and CO, as well as water, hydrogen, or hydrocarbons are present [58–62]. It remains unclear whether this reaction occurs directly at the metal particles or if H_2 dissociates on platinum, followed by hydrogen atom migration to the NCO species. Nevertheless, the temporal evolution of the Pt–CO band suggests that –NCO hydrolysis involves dissociation into N and CO, as indicated by the rapid saturation of Pt particles with CO and the subsequent transition to Pt–H once most –NCO species have decomposed (cf. Fig. 9). Notably, no additional CO or CO_2 is detected in the gas phase during the reaction with H_2. Both species originate from the preceding reactive deposition of –NCO and are purged from the system upon switching from the NO/CO mixture to H_2/N_2. However, the limited catalyst amount and the low temporal resolution of the gas phase FTIR measurements at the DRIFTS cell outlet must be considered, as these factors hinder reliable detection. Accurate identification and quantification of decomposition products would require complementary experiments employing larger catalyst amounts and higher temporal resolution, analogous to the powder bed studies.

A key observation is that the presence of NO or O_2 does not affect the decomposition rate of –NCO. The comparable rates under inert conditions and in the presence of oxidizing agents indicate that, at least over Pt/Al_2O_3, NCO decomposition proceeds primarily via thermal pathways, consistent with the findings of [29]. This result appears to contradict the assumption that isocyanate reacts with NO or O_2 to produce N_2, CO_2, and possibly N_2O [11, 52, 63–65], albeit at a significantly slower rate than its reaction with H_2 or H_2O [11, 29, 52, 59, 61, 62]. Conversely, the low reactivity of isocyanate toward oxidizing agents, combined with its high reactivity toward H_2 and H_2O, supports the existence of a reaction pathway leading to NH_3, with NCO acting as a key intermediate. Further experimental investigations are required to elucidate the detailed reaction pathways and confirm the mechanistic role of –NCO under varying conditions. In particular, the presence of H_2O and hydrocarbons are expected to strongly influence –NCO dynamics by providing additional hydrogen sources and surface intermediates that can compete with, or facilitate, isocyanate formation and consumption. Water can promote hydrolysis or hydrogenation pathways that accelerate –NCO conversion to NH_3. Systematic studies that explicitly include H_2O and representative hydrocarbons under multi-component feed conditions would therefore bridge the gap between idealized experiments and realistic exhaust gas compositions, enabling a more accurate assessment of the relevance of –NCO-mediated pathways under practical operating conditions.

5 Conclusion

Time-resolved studies in a powder bed reactor combined with *operando* DRIFTS measurements were conducted to explore how isocyanate species (–NCO) affect the performance of Pt/Al_2O_3 catalysts during NO reduction by CO. The decline in catalytic activity closely parallels the accumulation of –NCO on the alumina support, both occurring on similar timescales, which suggests a mechanistic connection or a shared underlying factor. While CO adsorption on Pt sites takes place nearly instantaneously and remains stable, –NCO formation is slower, strongly influenced by temperature and stoichiometry, and increases with CO coverage, confirming an equilibrium between –NCO concentration and gas phase composition.

Isocyanate is highly stable under oxidizing conditions, showing negligible reactivity toward NO or O_2 and decomposes primarily through thermal pathways. In contrast, the presence of hydrogen triggers rapid NCO decomposition, producing ammonia and water, revealing a fast route to NH_3 formation under exhaust conditions where H_2 or hydrocarbons coexist. These insights underscore the need to integrate NCO formation and decomposition into kinetic models for NO + CO reactions, as they significantly impact catalyst behavior and emissions control strategies. Overall, the study provides quantitative evidence of –NCO storage dynamics and its role in reversible deactivation, offering a basis for improved catalyst design in robust emission control systems.

Appendix A Transmission Electron Microscopy results

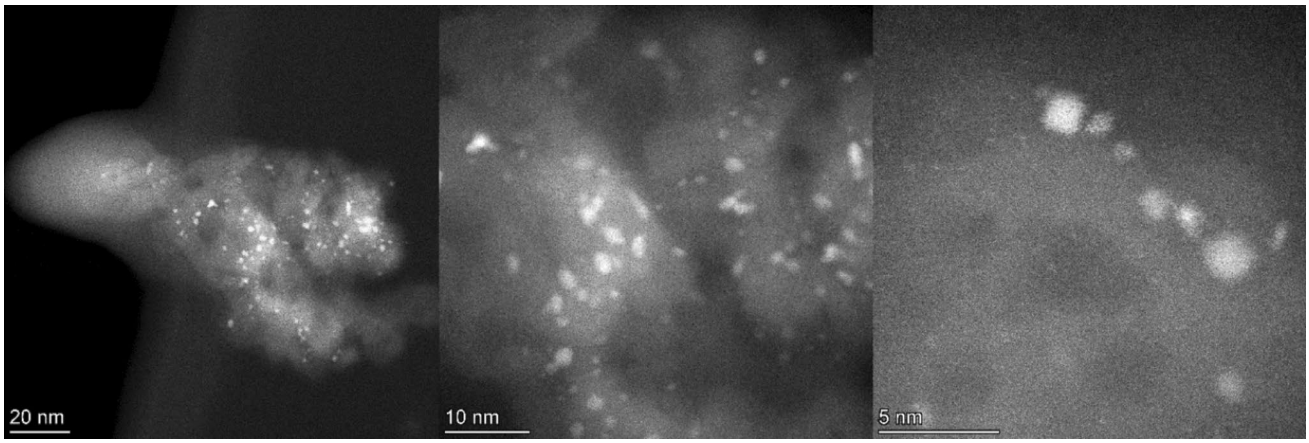

Fig. 11 Representative TEM images of the calcined Pt/Al_2O_3 catalyst showing a homogenous Pt dispersion over the Al_2O_3 surface as well as a narrow particle size distribution of Pt (bright spots). The particle size was determined using FIJI [67] by measuring the largest diameter of shown nanoparticles for a statistically significant amount of nanoparticles

Appendix B Powder Bed Reactor

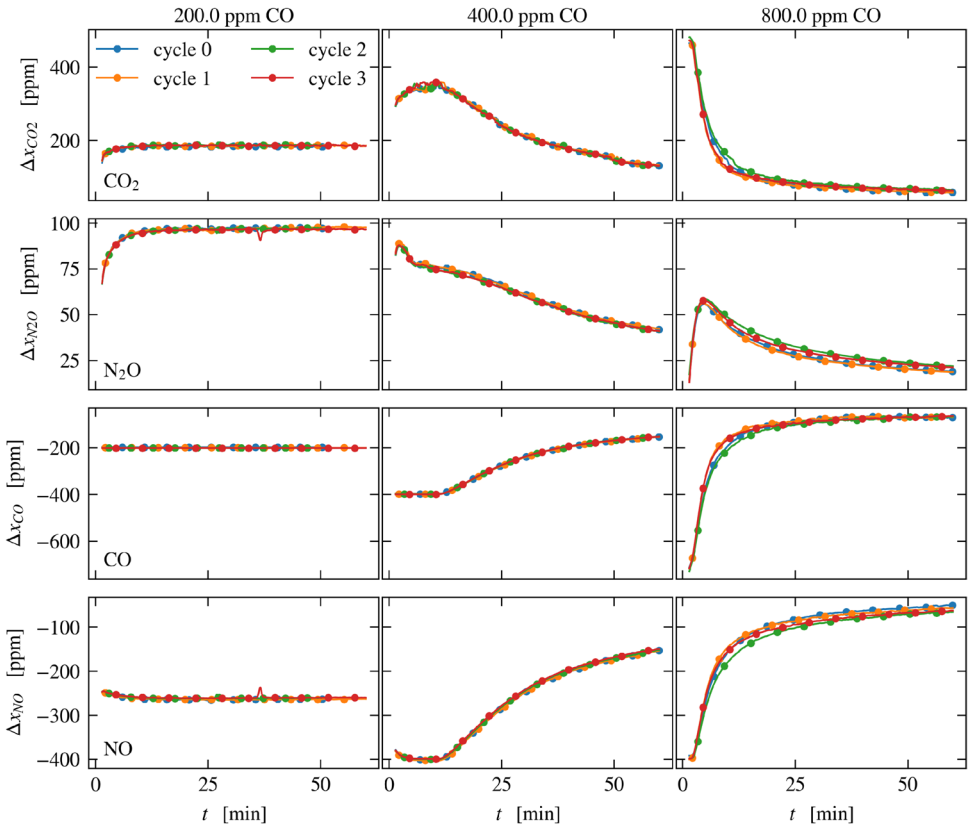

Fig. 12 Evolvement of the species concentrations over four consecutive catalytic cycles in the powder bed reactor (PBR) at 300°C for three different stoichiometries: net oxidizing (200 ppm CO), stoichiometric (400 ppm CO) and net reducing (800 ppm CO). Total gas flow (1.0L/min) and inlet NO concentration (400 ppm) are kept constant in all cases

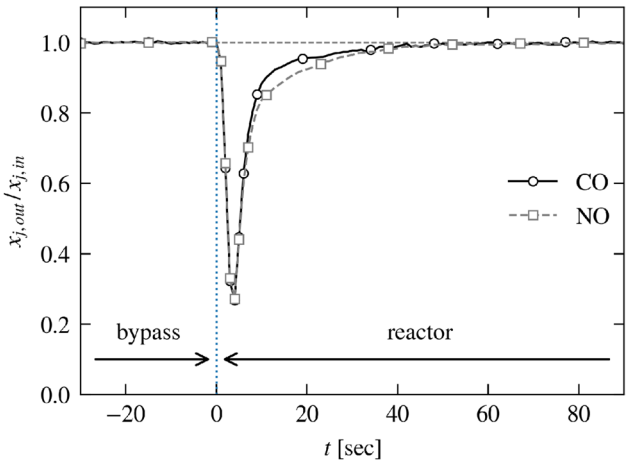

Fig. 13 Response time of the analytics to a sudden change of the inlet gas composition in the powder bed reactor without catalyst and at 300° C. Initially, NO and CO flow through the FTIR gas cell via a bypass while the reactor is maintained under nitrogen. Pneumatically actuated valves switch the gas flow from the bypass to the reactor. Decrease of concentrations as nitrogen is forced out of the reactor through the FTIR and is eventually replaced by the inlet gas mixture. After a maximum of about 50 to 60 s, all nitrogen in the entire system is replaced by the reactive gas mixture

Drifts

Figure 14 shows typical DRIFT spectra for the three different stoichiometries and for different temperatures in the region 1300 cm^{-1} to 2400 cm^{-1} obtained after 8 min. The intensity of the -NCO depends strongly on temperature and stoichiometry. With an excess of CO (800 ppm) is Pt-CO band, as an indicator of the CO coverage, is almost independent of temperature, while it significantly decreases with increasing temperature at 400 and 200 ppm. Figure 15 shows the same spectra, but normalized to the maximum intensity of the -NCO band to highlight the strong correlation between the nitrite/nitrate bands and the intense band of isocyanate. The same is true for the depletion of the free OH group and the formation of H-bonded OH groups (not shown here for brevity).

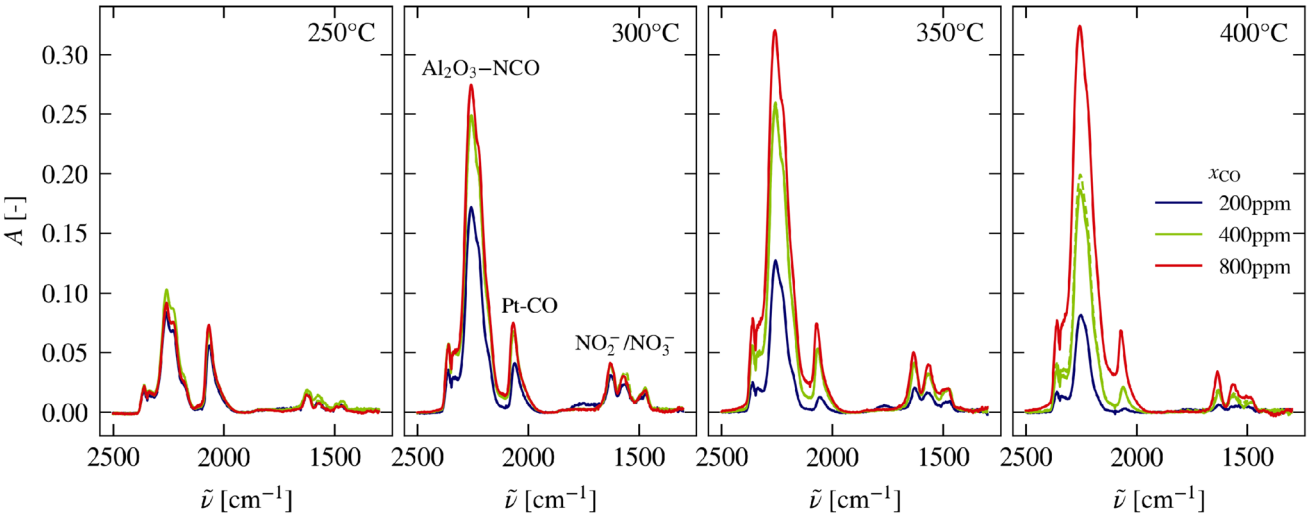

Fig. 14 IR spectra obtained 8 min after introducing the NO/CO mixture to the DRIFTS cell. (400 ppm NO, 250 mL/min)

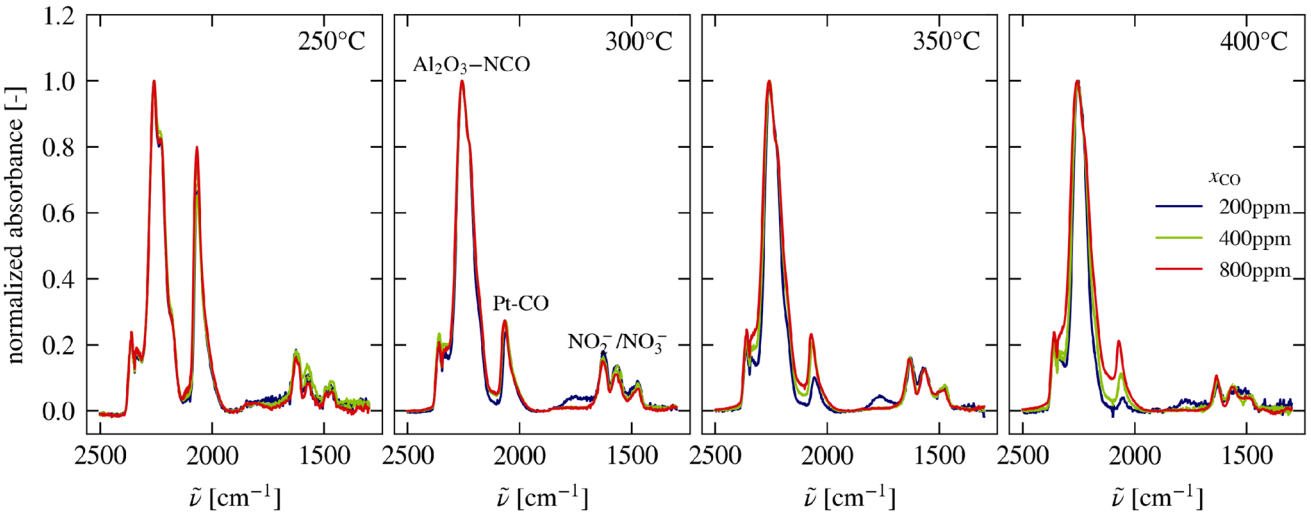

Fig. 15 IR spectra obtained 8 min after introducing the NO/CO mixture to the DRIFTS cell. All spectra are normalized to peak intensity of the -NCO band at 2261 cm^{-1}. (400 ppm NO, 250 mL/min)

Acknowledgements The financial support of the German Research Foundation (DFG) in the framework of the Collaborative Research Center 1441 (Project-ID 426888090) as well as the Helmholtz program "Materials and Technologies for the Energy Transition, Germany" (MTET, 38.03.04) is gratefully acknowledged. This work was performed with the help of the Large-Scale Data Facility (LSDF) at the Karlsruhe Institute of Technology funded by the Ministry of Science, Research and the Arts Baden-Württemberg and by the Federal Ministry of Education and Research. Graphics were prepared with the help of the Matplotlib Python package [66]. The authors thank Maria Casapu (ITCP, KIT), head of the catalyst preparation team in the CRC 1441, for helpful discussions, Joachim Czechowsky (ITCP, KIT) for the preparation of the catalysts, Daniel Hodonj and Wang Tao for support during the DRIFTS measurements, Thomas Bergfeldt (IAM-AWP, KIT) for the ICP-OES measurements and Carina B. Maliakkal (INT, KIT) for the TEM analysis.

Author Contributions T.H.: Investigation, Validation, Data Curation, Formal Analysis, Writing Original Draft, Visualization, Conceptualization S.S.: Investigation, Data Curation, Writing - Review & Editing L.C.: Investigation, Writing - Review & Editing S.W.: Investigation, Formal Analysis F.M.: Validation, Conceptualization, Writing - Review & Editing P.L.: Conceptualization, Validation, Writing - Review & Editing A.N.: Conceptualization, Validation, Formal Analysis, Supervision, Writing - Review & Editing C.W.: Resources, Funding acquisition J.D.G.: Resources, Funding acquisition, Supervision, Writing - Review & Editing O.D.: Resources, Funding acquisition, Supervision, Writing - Review & Editing

Funding Open Access funding enabled and organized by Projekt DEAL.

Data Availability Data sets presented in the current study will be made available at https://doi.org/10.35097/cu86hq6209xhnmu0.

Declarations

Competing Interests The authors declare no competing interests.

References

1. Forster, P., Ramaswamy, V., Artaxo, P., Berntsen, T., Betts, R., Fahey, D.W., Haywood, J., Lean, J., Lowe, D.C., Raga, G., Schulz, M., Dorland, R.V.: Changes in atmospheric constituents and in radiative forcing. In: Solomon, S., Qin, D., Manning, M., Chen, Z., Marquis, M., Averyt, K.B., Tignor, M., Miller, H.L. (eds.) Climate change 2007: The physical science basis. Contribution of working group I to the fourth assessment report of the intergovernmental panel on climate change. Cambridge University Press, Cambridge, United Kingdom and New York, NY, USA (2007)
2. Votsmeier, M., Kreuzer, T., Gieshoff, J., Lepperhoff, G., Elvers, B.: Automobile exhaust control. In: Ullmann's Encyclopedia of Industrial Chemistry, pp. 1–19. John Wiley & Sons, Ltd, Weinheim, Germany (2019). https://doi.org/10.1002/14356007.a03_189.pub3
3. Gholami, Z., Luo, G., Gholami, F., Yang, F.: Recent advances in selective catalytic reduction of NO_x by carbon monoxide for flue gas cleaning process: A review. Catalysis Reviews. **63**(1), 68–119 (2021). https://doi.org/10.1080/01614940.2020.1753972
4. Liu, Z., Yu, F., Ma, C., Dan, J., Luo, J., Dai, B.: A Critical Review of Recent Progress and Perspective in Practical Denitration Application. Catalysts **9**(9), 771 (2019). https://doi.org/10.3390/catal9090771

5. Xu, Z., Li, Y., Lin, Y., Zhu, T.: A review of the catalysts used in the reduction of NO by CO for gas purification. Environ. Sci. Pollut. Res. **27**(7), 6723–6748 (2020). https://doi.org/10.1007/s11356-019-07469-w
6. Granger, P., Dujardin, C., Paul, J.-F., Leclercq, G.: An overview of kinetic and spectroscopic investigations on three-way catalysts: Mechanistic aspects of the CO + NO and CO + N_2O reactions. J. Mol. Catal. A: Chem. **228**(1), 241–253 (2005). https://doi.org/10.1016/j.molcata.2004.09.081
7. Granger, P., Dhainaut, F., Pietrzik, S., Malfoy, P., Mamede, A.S., Leclercq, L., Leclercq, G.: An overview: Comparative kinetic behaviour of Pt, Rh and Pd in the NO+CO and NO+H_2 reactions. Top. Catal. **39**(1), 65–76 (2006). https://doi.org/10.1007/s11244-006-0039-0
8. Srinivasan, A., Depcik, C.: Review of Chemical Reactions in the NO Reduction by CO on Rhodium/Alumina Catalysts. Catalysis Reviews. **52**(4), 462–493 (2010). https://doi.org/10.1080/01614940.2010.522485
9. Fisher, G.B., Zammit, M.G., Labarge, W.J.: Investigation of catalytic alternatives to rhodium in emissions control. SAE Technical Paper. **920846** (1992). https://doi.org/10.4271/920846
10. Matthey, J.: PGM Market Report 2022 (2022). https://matthey.com/pgm-market-report-2022
11. Unland, M.L.: Isocyanate intermediates in the reaction nitrogen monoxide + carbon monoxide over a platinum/aluminum oxide catalyst. J. Phys. Chem. **77**(16), 1952–1956 (1973). https://doi.org/10.1021/j100635a006
12. Srinivasan, A., Depcik, C.: Review of chemical reactions in the NO reduction by CO on platinum/alumina catalysts. Surf. Rev. Lett. **19**(01), 1230001 (2012). https://doi.org/10.1142/S0218625X12300018
13. Mantri, D., Aghalayam, P.: Detailed surface reaction mechanism for reduction of NO by CO. Catal. Today **119**(1), 88–93 (2007). https://doi.org/10.1016/j.cattod.2006.08.002
14. Frank, B., Renken, A.: Kinetics and deactivation of the NO reduction by CO on Pt-supported catalysts. Chem. Eng. Technol. **22**(6), 490–494 (1999). https://doi.org/10.1002/(SICI)1521-4125(199906)22:6U+3C490::AID-CEAT490U+3E3.0.CO;2-9
15. Granger, P., Dathy, C., Lecomte, J.J., Leclercq, L., Prigent, M., Mabilon, G., Leclercq, G.: Kinetics of the NO and CO Reaction over Platinum Catalysts: I. Influence of the Support. J. Catal. **173**(2), 304–314 (1998). https://doi.org/10.1006/jcat.1997.1932
16. Banholzer, W.F., Masel, R.I.: A reflection-absorption infrared study of carbon monoxide and nitric oxide adsorption on platinum (100). Surf. Sci. **137**(1), 339–360 (1984). https://doi.org/10.1016/0039-6028(84)90694-0
17. Gorte, R.J., Schmidt, L.D., Sexton, B.A.: The electron energy loss spectrum of isocyanic acid on the Pt(111) surface. J. Catal. **67**(2), 387–391 (1981). https://doi.org/10.1016/0021-9517(81)90298-0
18. Lesley, M.W., Schmidt, L.D.: The NO + CO reaction on Pt(100). Surf. Sci. **155**(1), 215–240 (1985). https://doi.org/10.1016/0039-6028(85)90415-7
19. Engel, T., Ertl, G.: Elementary Steps in the Catalytic Oxidation of Carbon Monoxide on Platinum Metals. In: Eley, D.D., Pines, H., Weez, P.B. (eds.) Advances in Catalysis vol. 28, pp. 1–78. Academic Press Inc., Cambridge, Massachusetts, USA (1979). https://doi.org/10.1016/S0360-0564(08)60133-9
20. Kobylinski, T.P., Taylor, B.W.: The catalytic chemistry of nitric oxide: II. Reduction of nitric oxide over noble metal catalysts. J. Catal. **33**(3), 376–384 (1974). https://doi.org/10.1016/0021-9517(74)90284-X
21. Muraki, H., Fujitani, Y.: Nitric oxide reduction by carbon monoxide over noble-metal catalysts under cycled feedstreams. Ind. Eng. Chem. Prod. Res. Develop. **25**(3), 414–419 (1986). https://doi.org/10.1021/i300023a008
22. Lorimer, D., Bell, A.T.: Reduction of NO by CO over a silica-supported platinum catalyst: Infrared and kinetic studies. J. Catal. **59**(2), 223–238 (1979). https://doi.org/10.1016/S0021-9517(79)80027-5
23. Pisanu, A.M., Gigola, C.E.: NO decomposition and NO reduction by CO over Pd/α-Al_2O_3. Appl. Catal. B **20**(3), 179–189 (1999). https://doi.org/10.1016/S0926-3373(98)00110-6
24. Sadhankar, R.R., Lynch, D.T.: NO Reduction by CO over a Pt/Al_2O_3 Catalyst: Reaction Kinetics and Experimental Bifurcation Behavior. Ind. Eng. Chem. Res. **36**(11), 4609–4619 (1997). https://doi.org/10.1021/ie970138z
25. Chang, C.C., Hegedus, L.L.: Surface reactions of NO, CO, and O_2 near the stoichiometric point: I. Pt-alumina. J. Catal. **57**(3), 361–371 (1979). https://doi.org/10.1016/0021-9517(79)90002-2
26. Freysz, J.-L., Saussey, J., Lavalley, J.-C., Bourges, P.: In Situ FTIR Study of the NO+CO Reaction on a Silica-Supported Platinum Catalyst at Atmospheric Pressure Using a New Pulse Technique. J. Catal. **197**(1), 131–138 (2001). https://doi.org/10.1006/jcat.2000.3060
27. Hegedus, L.L., Chang, C.C., McEwen, D.J., Sloan, E.M.: Response of Catalyst Surface Concentrations to Forced Concentration Oscillations in the Gas Phase. The NO, CO, O_2 System over Pt-Alumina. Ind. Eng. Chem. Fund. **19**(4), 367–373 (1980). https://doi.org/10.1021/i160076a008
28. Mergler, Y.J., Nieuwenhuys, B.E.: NO Reduction by CO over Pt/Al_2O_3 and Pt/CeO_x/Al_2O_3: Oscillations and Deactivation. J. Catal. **161**(1), 292–303 (1996). https://doi.org/10.1006/jcat.1996.0187
29. Niiyama, H., Tanaka, M., Iida, H., Echigoya, E.: Infrared Studies of the Isocyanate Species Formed in the Reaction of NO with CO over Pt and Rh. Bull. Chem. Soc. Jpn. **49**(8), 2047–2050 (1976). https://doi.org/10.1246/bcsj.49.2047
30. Solymosi, F., Völgyesi, L., Sárkány, J.: The effect of the support on the formation and stability of surface isocyanate on platinum. J. Catal. **54**(3), 336–344 (1978). https://doi.org/10.1016/0021-9517(78)90081-7
31. Xiao, P., Davis, R.C., Ouyang, X., Li, J., Thomas, A., Scott, S.L., Zhu, J.: Mechanism of NO reduction by CO over Pt/SBA-15. Catal. Commun. **50**, 69–72 (2014). https://doi.org/10.1016/j.catcom.2014.02.027
32. Solymosi, F., Kiss, J., Sarkany, J.: On the reactions of surface isocyanate over platinum catalyst. In: Proceedings 3rd International Conference on Solid Surfaces, **1**, 819–822 (1977)
33. Solymosi, F., Sárkány, J., Schauer, A.: Study of the formation of isocyanate surface complexes on Pt/Al_2O_3 catalysts. J. Catal. **46**(3), 297–307 (1977). https://doi.org/10.1016/0021-9517(77)90213-5
34. Chilukoti, S., Widjaja, E., Gao, F., Zhang, H., Anderson, B.G., Niemantsverdriet, J.W.H., Garland, M.: Spectral reconstruction of surface adsorbed species using band-target entropy minimization. Application to CO and NO reaction over a Pt/γ-Al_2O_3 catalyst using in situ DRIFT spectroscopy. Phys. Chem. Chem. Phys. **10**(24), 3535–3547 (2008). https://doi.org/10.1039/B714544F
35. Häber, T., Wan, S., Struzek, S., Cárdenas, C., Zimina, A., Maurer, F., Lott, P., Suntz, R., Grunwaldt, J.-D., Deutschmann, O.: Novel advanced channel reactor for spatio-temporal activity and catalyst state correlations applied for the reduction of NO by CO over Pt/Al_2O_3. Applied Catalysis A: General, 120748 (2025). https://doi.org/10.1016/j.apcata.2025.120748
36. Kleist, W., Grunwaldt, J.-D.: High output catalyst development in heterogeneous gas phase catalysis. In: Hagemeyer, A., Volpe, A. (eds.) Modern Applications of High Throughput R&D in Heterogeneous Catalysis, pp. 357–371. Bentham Science Publishers (2014). https://doi.org/10.2174/9781608058723114010018
37. Maurer, F., Jelic, J., Wang, J., Gänzler, A., Dolcet, P., Wöll, C., Wang, Y., Studt, F., Casapu, M., Grunwaldt, J.-D.: Tracking the formation, fate and consequence for catalytic activity of Pt single

sites on CeO_2. Nat. Catal. **3**(10), 824–833 (2020). https://doi.org/10.1038/s41929-020-00508-7
38. Bergeret, G., Gallezot, P.: Particle size and dispersion measurements. In: Handbook of Heterogeneous Catalysis, pp. 738–765. John Wiley & Sons, Ltd, Weinheim, Germany (2008). Chap. 3.1.2. https://doi.org/10.1002/9783527610044.hetcat0038
39. Caulfield, L., Sauter, E., Idriss, H., Wöll, C.: Tracking the redox properties of CeO_2 powders by infrared spectroscopy: Monitoring the defect states by O_2 adsorption and the Ce_{3+} spin-orbit transition. J. Phys. Chem. C **129**(2), 1228–1233 (2025). https://doi.org/10.1021/acs.jpcc.4c07816
40. Chen, S., Pleßow, P.N., Yu, Z., Sauter, E., Caulfield, L., Nefedov, A., Studt, F., Wang, Y., Wöll, C.: Structure and chemical reactivity of Y-stabilized ZrO_2 surfaces: Importance for the water-gas shift reaction. Angew. Chem. Int. Ed. **63**(27), 202404775 (2024). https://doi.org/10.1002/anie.202404775
41. Struzek, S., Delrieux, T., Maurer, F., Gonçalves, D.S., Heck, S.-L., Klag, L., Czechowsky, J., Zimina, A., Grunwaldt, J.-D.: Role of powders and coatings for relating catalytic activity and structure of Pt in emission control catalysis. Reaction Chemistry & Engineering. **10**(6), 1233–1243 (2025). https://doi.org/10.1039/D4RE00262H
42. Kecskeméti, A., Bánsági, T., Solymosi, F.: Formation and Migration of NCO Species on Ag/SiO_2 Catalyst. Catal. Lett. **116**(3), 101–104 (2007). https://doi.org/10.1007/s10562-007-9153-2
43. Solymosi, F., Völgyesi, L., Raskó, J.: The Effects of Different Supports on the Formation and Reactivity of Surface Isocyanate on Pd, Ir, Ru and Rh. Z. Phys. Chem. **120**(1), 79–87 (1980). https://doi.org/10.1524/zpch.1980.120.1.079
44. Raskó, J., Solymosi, F.: Infrared study of the formation and stability of isocyanate species on some unsupported noble metals. J. Catal. **71**(1), 219–222 (1981). https://doi.org/10.1016/0021-9517(81)90220-7
45. Jones, J.E., Trenary, M.: Surface Chemistry of NCO Formed from HNCO on Pt(111). The Journal of Physical Chemistry C. **112**(51), 20443–20450 (2008). https://doi.org/10.1021/jp807906e
46. Solymosi, F., Kiss, J.: Adsorption and surface dissociation of HNCO on Pt(110) surfaces: LEED, AES. ELS and TDS studies. Surface Science. **108**(3), 641–659 (1981). https://doi.org/10.1016/0039-6028(81)90570-7
47. Giechaskiel, B., Clairotte, M.: Fourier transform infrared (FTIR) spectroscopy for measurements of vehicle exhaust emissions: A review. Appl. Sci. **11**(16), 7416 (2021). https://doi.org/10.3390/app11167416
48. Barreau, M., Courtois, X., Can, F.: FT-IR spectroscopy study of HNCO adsorption and hydrolysis over oxide-based samples dedicated to deNO_x processes. Applied Catalysis A: General. **552**, 147–153 (2018) https://doi.org/10.1016/j.apcata.2017.12.019
49. Wang, J., Sauter, E., Nefedov, A., Heißler, S., Maurer, F., Casapu, M., Grunwaldt, J.-D., Wang, Y., Wöll, C.: Dynamic Structural Evolution of Ceria-Supported Pt Particles: A Thorough Spectroscopic Study. J. Phys. Chem. C **126**(21), 9051–9058 (2022). https://doi.org/10.1021/acs.jpcc.2c02420
50. Liu, X., Truitt, R.E.: DRFT-IR studies of the surface of γ-alumina. J. Am. Chem. Soc. **119**(41), 9856–9860 (1997). https://doi.org/10.1021/ja971214s
51. Liu, X.: DRIFTS study of surface of γ-alumina and its dehydroxylation. J. Phys. Chem. C **112**(13), 5066–5073 (2008). https://doi.org/10.1021/jp711901s
52. Ji, Y., Toops, Todd.J., Crocker, M.: Isocyanate formation and reactivity on a Ba-based LNT catalyst studied by DRIFTS. Appl. Catal. B: Environ. **140–141**, 265–275 (2013). https://doi.org/10.1016/j.apcatb.2013.04.017
53. Sirita, J., Phanichphant, S., Meunier, F.C.: Quantitative Analysis of Adsorbate Concentrations by Diffuse Reflectance FT-IR. Anal. Chem. **79**(10), 3912–3918 (2007). https://doi.org/10.1021/ac0702802
54. Sage, D., Donati, L., Soulez, F., Fortun, D., Schmit, G., Seitz, A., Guiet, R., Vonesch, C., Unser, M.: DeconvolutionLab2: An open-source software for deconvolution microscopy. Methods **115**, 28–41 (2017). https://doi.org/10.1016/j.ymeth.2016.12.015
55. Ravasi, M., Vasconcelos, I.: PyLops - A linear-operator Python library for scalable algebra and optimization. Softwarex. **11**, 100361 (2020). https://doi.org/10.1016/j.softx.2019.100361
56. Rodrigues, A.E.: Residence time distribution (RTD) revisited. Chem. Eng. Sci. **230**, 116188 (2021). https://doi.org/10.1016/j.ces.2020.116188
57. Carosso, M., Vottero, E., Lazzarini, A., Morandi, S., Manzoli, M., Lomachenko, K.A., Ruiz, M.J., Pellegrini, R., Lamberti, C., Piovano, A., Groppo, E.: Dynamics of reactive species and reactant-induced reconstruction of Pt clusters in Pt/Al_2O_3 catalysts. ACS Catal. **9**(8), 7124–7136 (2019). https://doi.org/10.1021/acscatal.9b02079
58. Solymosi, F., Sárkány, J.: Study of the formation and reactivity of surface isocyanate on Pd/Al_2O_3 catalysts. React. Kinet. Catal. Lett. **3**(3), 297–299 (1975). https://doi.org/10.1007/BF02067769
59. Cant, N.W., Angove, D.E., Chambers, D.C.: Nitrous oxide formation during the reaction of simulated exhaust streams over rhodium, platinum and palladium catalysts. Appl. Catal. B **17**(1), 63–73 (1998). https://doi.org/10.1016/S0926-3373(97)00105-7
60. Macleod, N., Lambert, R.M.: An in situ DRIFTS study of efficient lean NOx reduction with H_2 + CO over Pd/Al_2O_3: The key role of transient NCO formation in the subsequent generation of ammonia. Appl. Catal. B **46**(3), 483–495 (2003). https://doi.org/10.1016/S0926-3373(03)00289-3
61. Szailer, T., Kwak, J.H., Kim, D.H., Hanson, J.C., Peden, C.H.F., Szanyi, J.: Reduction of stored NOx on Pt/Al_2O_3 and $Pt/BaO/Al_2O_3$ catalysts with H_2 and CO. J. Catal. **239**(1), 51–64 (2006). https://doi.org/10.1016/j.jcat.2006.01.014
62. Can, F., Courtois, X., Royer, S., Blanchard, G., Rousseau, S., Duprez, D.: An overview of the production and use of ammonia in NSR + SCR coupled system for NOx reduction from lean exhaust gas. Catal. Today **197**(1), 144–154 (2012). https://doi.org/10.1016/j.cattod.2012.07.032
63. Bae, W.B., Kim, D.Y., Byun, S.W., Hazlett, M., Yoon, D.Y., Jung, C., Kim, C.H., Kang, S.B.: Emission of NH_3 and N_2O during NO reduction over commercial aged three-way catalyst (TWC): Role of individual reductants in simulated exhausts. Chem. Eng. J. Adv. **9**, 100222 (2022). https://doi.org/10.1016/j.ceja.2021.100222
64. Lesage, T., Verrier, C., Bazin, P., Saussey, J., Daturi, M.: Studying the NOx-trap mechanism over a $Pt-Rh/Ba/Al_2O_3$ catalyst by operando FT-IR spectroscopy. Phys. Chem. Chem. Phys. **5**(20), 4435–4440 (2003). https://doi.org/10.1039/B305874N
65. Castoldi, L., Matarrese, R., Kubiak, L., Daturi, M., Artioli, N., Pompa, S., Lietti, L.: In-depth insights into N_2O formation over Rh- and Pt-based LNT catalysts. Catal. Today **320**, 141–151 (2019). https://doi.org/10.1016/j.cattod.2018.01.026
66. Hunter, J.D.: Matplotlib: A 2D Graphics Environment. Comput. Sci. Eng. **9**(3), 90–95 (2007). https://doi.org/10.1109/MCSE.2007.55
67. Schindelin, J., Arganda-Carreras, I., Frise, E., Kaynig, V., Longair, M., Pietzsch, T., Preibisch, S., Rueden, C., Saalfeld, S., Schmid, B., Tinevez, J.-Y., White, D.J., Hartenstein, V., Eliceiri, K., Tomancak, P., Cardona, A.: Fiji: An open-source platform for biological-image analysis. Nat. Methods **9**(7), 676–682 (2012). https://doi.org/10.1038/nmeth.2019